Using an oxidation flow reactor to understand the effects of gasoline aromatics and ethanol levels on secondary aerosol formation

Niina Kuittinen[1,2], Cavan McCaffery[2], Stephen Zimmerman[3], Roya Bahreini[3,*], Pauli Simonen[1], Panu Karjalainen[1], Jorma Keskinen[1], Topi Rönkkö[1], Georgios Karavalakis[2,4,*]

[1]Aerosol Physics Laboratory, Physics Unit, Faculty of Engineering and Natural Sciences, Tampere University, Tampere, FI-33720, Finland

[2]University of California, Bourns College of Engineering, Center for Environmental Research and Technology (CE-CERT), 1084 Columbia Avenue, Riverside, CA 92507, USA

[3]Department of Environmental Sciences, University of California, Riverside, 900 University Avenue, Riverside, CA 92521

[4]Department of Chemical and Environmental Engineering, Bourns College of Engineering, University of California, Riverside, CA 92521, USA

Abstract

Fuel type and composition affect tailpipe emissions and secondary aerosol production from mobile sources. This study assessed the influence of gasoline fuels with varying levels of aromatics and ethanol on the primary emissions and secondary aerosol formation from a flexible fuel vehicle equipped with a port fuel injection engine. The vehicle was exercised over the LA92 and US06

* Corresponding Authors. Georgios Karavalakis, E-mail address: gkaraval@cert.ucr.edu

Roya Bahreini, E-mail address: bahreini@ucr.edu

driving cycles using a chassis dynamometer. Secondary aerosol formation potential was measured using a fast oxidation flow reactor. Results showed that the high aromatics fuels led to higher gaseous regulated emissions, as well as particulate matter (PM), black carbon, and total and solid particle number. The high ethanol content fuel (E78) resulted in reductions for the gaseous regulated pollutants and particulate emissions. Secondary aerosol formation potential was dominated by the cold-start phase and increased for the high aromatics fuel. Secondary aerosol formation was seen in lower levels for E78 due to the lower formation of precursor emissions using this fuel. In addition, operating driving conditions and aftertreatment efficiency played a major role on secondary organic and inorganic aerosol formation, indicating that fuel properties, driving conditions, and exhaust aftertreatment should be consider when evaluating the emissions of secondary aerosol precursors from mobile sources.

Keywords: Secondary organic aerosol (SOA); ethanol blends; gasoline aromatics; oxidation flow reactor

1. Introduction

Secondary organic aerosol (SOA) is formed from the oxidation of diverse non-methane organic gases (NMOGs), ranging in volatility from volatile to intermediate volatility and semivolatile organic compounds (VOCs, IVOCs, and SVOCs, respectively) and comprising a large fraction of the total ambient organic aerosol mass (Jimenez et al., 2009). SOA is known to affect climate change, air quality, and public health (Kanakidou et al., 2005; Tuet et al., 2017). Gasoline motor vehicles are important sources of NMOGs of different volatility classes resulting from incomplete combustion, including aromatic VOCs and long-chain alkanes, which favor the formation of SOA (Derwent et al., 2010; Drozd et al., 2019; Zhao et al., 2018). It has been previously reported that

gasoline vehicles are significant contributors to urban SOA budget and a more dominant source than diesel vehicles (Bahreini et al., 2012a; Platt et al., 2017). A number of studies have demonstrated elevated SOA formation from gasoline vehicle exhaust using smog chambers and flow reactors, with the amount of SOA formed substantially exceeding primary organic aerosol (POA) emissions (Vu et al., 2019; Roth et al., 2019; Nordin et al., 2013; Du et al., 2018; Karjalainen et al., 2016).

Primary emissions and SOA formation from precursors emitted by motor vehicles can be significantly affected by gasoline composition and properties (Yang et al., 2019a; Yang et al., 2019b; Fushimi et al., 2016; Peng et al., 2017; Roth et al., 2020a). The widespread use of ethanol, the biofuel of choice in the United States (US), Europe, and other parts of the world, has been shown to reduce most harmful emissions from gasoline vehicles that have historically utilized multipoint port fuel injection (PFI) systems and in vehicles with the more efficient gasoline direct injection (GDI) engines (Karavalakis et al., 2014a; Maricq et al., 2012; Hays et al., 2013; Durbin 2007; Clairotte et al., 2013; Timonen et al., 2017). In particular, higher ethanol concentrations used in flexible fuel vehicles (FFVs) designed to run with any ethanol blend up to 83% have been shown to offer large reductions in particulate matter (PM) and black carbon emissions, as well as reductions in mobile source air toxic pollutants, such as benzene, toluene, ethylbenzene, xylenes (BTEX), and polycyclic aromatic hydrocarbons (PAHs) (Karavalakis et al., 2014b; Suarez-Bertoa et al., 2015a; Yang et al., 2019c; McCaffery et al., 2020; Jin et al., 2017; Timonen et al., 2017). Other studies have also demonstrated that the total content and volatility distribution of aromatic hydrocarbons in gasoline will influence tailpipe emissions (Fushimi et al., 2016; Yang et al., 2019a; Yao et al., 2017). High molecular weight and less volatile aromatic hydrocarbons will promote the formation of a wide volatility range organic compounds (i.e., semivolatile and

intermediate volatility) and primary PM emissions during combustion, and especially during cold-start conditions (Fushimi et al., 2016; Yang et al., 2019a; Yang et al., 2019b; Aikawa et al., 2010).

While considerable attention has been received on the impacts of fuel composition on primary emissions, little is known on the fuel effects on secondary aerosol formation from gasoline vehicles. In addition, the extent to which fuel composition and properties affect SOA formation is not always clear. Studies have looked into the direct evaporation of fuels to better understand the effect of fuel properties on SOA formation (Jathar et al., 2013; He et al., 2020). While this approach is useful, it often neglects the complex combustion processes, including the formation pathways of SOA precursors that are not necessarily present in the fuel in considerable amounts, or the potential interactions of fuel properties that can affect emissions of these species. Roth et al. (2020a) and Yang et al. (2019a) showed that match-blended ethanol fuels in low concentrations with high levels of heavier aromatics will likely increase VOC precursor emissions from GDI vehicles operated on the LA92 cycle, and subsequently SOA production due to the higher heat of vaporization of ethanol, which will lead to cooling of the cylinder environment, slowing fuel evaporation and increasing fuel impingement. Peng et al. (2017) also reported that gasoline fuels with higher aromatic levels will increase VOC precursor emissions and contribute to higher SOA production when they introduced the exhausts of PFI and GDI vehicles into an environmental chamber. Different studies, however, utilizing higher ethanol blends have reported reductions in SOA production from FFVs (Suarez-Bertoa et al., 2015b; Roth et al., 2020b; Gramsch et al., 2018; Timonen et al., 2017). For example, Roth et al. (2020b) proposed that the oxygen content and the dilution of aromatics in E30 and E78 blends were the dominant factors for the lower precursor emissions and the reduced SOA formation from the aged emissions from two FFVs operated over the LA92 cycle when introduced into an environmental chamber. Similarly, Timonen et al. (2017)

found reductions in precursor emissions and SOA formation as the ethanol content increased from E10 to E85 and E100 on an FFV operated over the New European Driving Cycle (NEDC) with the use of a potential aerosol mass (PAM) reactor.

Similar to traditional large-volume chambers, oxidation flow reactors (OFRs) have been recently employed as an alternative approach for the evaluation of real-time SOA formation (Kang et al., 2007; Lambe et al., 2011). While numerous studies utilized OFRs to investigate SOA formation from motor vehicles (Kuittinen et al., 2021; Cao et al., 2020; Simonen et al., 2019; Pieber et al., 2018; Karjalainen et al., 2016; Zhao et al., 2018), there is only a single vehicle study using an OFR that investigated the effects of ethanol blending on SOA formation (Timonen et al., 2017). The purpose of this study is the transient characterization of the potential for secondary aerosol formation from exhaust emitted by a modern PFI FFV fueled with two E10 fuels with different aromatic contents and a E78 blend when operated over the LA92 and US06 cycles. This study also reports the primary gaseous and particulate emissions, as well as the secondary aerosol formation potential as a function of fuel type and driving conditions.

2. Experimental

2.1 Vehicle and driving cycles

A 2017 model year light-duty vehicle with a flex fuel 3.6-liter, 6-cylinder, naturally-aspirated port fuel injection, spark ignition engine was employed in this study. The engine had a rated horsepower of 283 hp at 6400 rpm, a torque of 260 ft-lbs. at 4400 rpm, and a compression ratio of 10.2:1. The vehicle was equipped with a three-way catalyst (TWC) and was certified under EPA Tier 3 B110 or California ULEVII emissions standards.

The vehicle was tested on each fuel over the LA92 and US06 cycles. The LA92 is a dynamometer driving schedule for light-duty vehicles developed by the California Air Resources Board (CARB). It consists of three phases or three bags representing cold-start, hot-running, and hot-start driving conditions. Average emissions data were calculated by incorporating weighting factors of 0.43, 1, and 0.43, respectively, for the representing cold-start, hot-running, and hot-start LA92 phases. The LA92 has a total distance of 9.8 miles and an average speed of 24.6 miles/hr. The US06 Supplemental Federal Test Procedure (SFTP or US06) was developed to reflect aggressive, high speed, and high acceleration driving behavior. It has a total distance of 8.01 miles with an average speed of 48.4 miles/hr. Testing on the LA92 cycle was performed as a cold-start, while testing on the US06 was a hot-start with two back-to-back preconditioning US06 cycles to ensure the engine was warmed up.

2.2 Test fuels

Three fuels were employed for this study that were manufactured and supplied by Gage Products Company (Ferndale, MI). The baseline fuel was a US EPA Tier 3 E10 fuel (denoted as E10) with total aromatics content of 28.1 vol %. A higher aromatic content E10 fuel (36.7 vol %) was used to compare the impact of aromatics on primary emissions and aged PM (hereinafter denoted as E10HA). The third fuel contained 78% of denatured ethanol (denoted as E78) and was blended following the US EPA Tier 3 and the CARB certification requirements for E85 fuels. The ethanol concentration of 78 vol % was selected to meet the ASTM D5798 Reid vapor pressure (RVP) target. The composition of each compound family for the test fuels is shown in Figure 1, while the main fuel properties are shown in Table SM1, Supplementary Material (SM).

2.3 Emissions testing

Emissions measurements were conducted in CE-CERT's Vehicle Emissions Research Laboratory (VERL), on a Burke E. Porter 48-inch single-roll electric dynamometer. A Pierburg Positive Displacement Pump-Constant Volume Sampling (PDP-CVS) system was used to obtain standard bag measurements for total hydrocarbons (THC), carbon monoxide (CO), nitrogen oxides (NOx), non-methane hydrocarbons (NMHC), and carbon dioxide (CO_2). Gaseous emissions were determined according to the US EPA protocols for light-duty emission testing as specified in the Code of Federal Regulations (CFR), Title 40, Part 86. Cumulative tailpipe PM mass emissions were measured following the procedures in 40 CFR 1065. Total particle number concentrations were measured using a TSI 3776 ultrafine-Condensation Particle Counter (CPC) with a 2.5 nm cut point. The instrument operated at a flowrate of 1.5 L/min. Solid particle number counts were measured with the use of a catalytic stripper. The particles were counted downstream of the catalytic stripper with a TSI 3776 ultrafine CPC at a flow rate of 1.5 L/min. An ejector diluter was used to collect particle number samples from the CVS tunnel. Particle size distributions were obtained using an Engine Exhaust Particle Sizer (EEPS) spectrometer. The EEPS (TSI 3090, firmware version 8.0.0) was used to obtain real-time second-by-second size distributions between 5.6 to 560 nm. Particles were sampled at a flow rate of 10 L/min, which is considered to be high enough to minimize diffusional losses.

2.4 Photooxidation experiments

Diluted exhaust (by dilution factors of ~200-350) from the vehicle was introduced into an oxidation flow reactor, which was designed and developed by Tampere University (hereinafter denoted as Tampere Secondary Aerosol Reactor or TSAR). More details about the TSAR are

shown elsewhere (Kuittinen et al., 2021; Simonen et al., 2019; Simonen et al., 2017), while details of the photooxidation setup are provided in SM. Briefly, the TSAR is an OFR254-type oxidation flow reactor that consists of a residence time chamber, an oxidation reactor, an ozone (O_3) generator, and an expansion tube connecting the residence time chamber and oxidation reactor. It was designed to measure potential secondary aerosol formation from rapidly changing emission sources, such as vehicle exhaust, and it is characterized by nearly laminar flow conditions. The vehicle exhaust combined with dilution by ozone and humidified air passes through the residence time chamber where it is exposed to 254 nm UV radiation, producing OH radicals from ozone photolysis. Precursors react with OH or O_3 to produce lower volatility molecules that then transfer to particle phase and produce secondary aerosol. The average photooxidation timescales (Table SM2) varied between 6.3 to 7.4 days of atmospheric aging, which are within the timescales previously found to simulate peak SOA formation (Kuittinen et al., 2021; Tkacik et al., 2014; Ortega et al., 2016). The modeled OH exposure for all fuel/cycle combinations within TSAR are shown in Figure SM1. The photooxidation and corresponding OH exposures were calculated with a chemical reaction model considering CO suppression in the TSAR (Simonen et al. 2017).

Size-fractionated mass concentration of aerosols downstream of TSAR was measured by an electrical low-pressure impactor (ELPI+, Dekati Ltd) at 1 Hz frequency while bulk composition of the non-refractory aerosols (organic aerosols or OA, sulfate, nitrate, and ammonium) was measured by a mini aerosol mass spectrometer, equipped with a compact time-of-flight detector (mAMS, Aerodyne Research, Inc.), at 7-8 s intervals (Jayne et al., 2000; Vu et al., 2016). Given the mass accuracy of < 20 ppm and mass resolution (i.e., $m/\Delta m$ with m being the nominal m/z and Δm the full- width at half-maximum) of ~1100, high-resolution analysis of raw spectra was carried out using Wavemetrics Igor Pro. (Squirrel ToF-AMS analysis toolkit v. 1.60 with PIKA module

1.20) to calculate the concentration of the inorganics (except ammonium), OA, and the main families of OA ($C_xH_y^+$, $C_xH_yO^+$, $C_xH_yO_{z>1}^+$) (Bahreini et al., 2012b). Given the variable concentration of CO_2 in the vehicle exhaust, gas-phase background CO_2 was subtracted from the OA mass spectra using the measured gas-phase CO_2 concentrations from the CVS and the recommendation by Collier and Zhang, (2013). A composition-dependent collection efficiency factor was used to correct for particle bounce on the vaporizer (Middlebrook et al., 2012). Concentrations of the hydrocarbon-like OA (HOA) were estimated based on a modification to the formula suggested by Ng et al. (2011) as outlined in Kuittinen et al. (2021), namely HOA∼ 13.4 × C_{C4H9}^+, where C_{C4H9}^+ is the concentration of the non-oxygenated, hydrocarbon-like ion at *m/z* 57. The remaining mass of OA was assigned as oxygenated and secondary OA (SOA).

3. Results and Discussion

3.1 Primary emissions over the LA92 and US06 cycles

Tailpipe gaseous and particulate emissions for the LA92 cycle are shown in Table 1. It was not possible to estimate the weighted emissions of E10 fuel over the LA92 cycle due to a failure in the chassis dynamometer controls during the hot-start phase (bag 3) of the LA92 cycle. However, fuel comparison can be made based on the cold-start phase (bag 1) emissions of the LA92 cycle. While difficult to paint a complete picture for the weighted LA92 results, cold-start phase showed higher THC, NMHC, CO, and NOx emissions for both E10HA and E78 fuels by factors of 1.5-4.7 and 4.2-6.8, respectively, compared to E10. Consistent with previous studies of PFI and GDI vehicles, THC, NMHC, and CO emissions will likely increase with higher aromatic content fuels (Zhu et al., 2017; Karavalakis et al., 2015; Yang et al., 2019a; Yang et al., 2019c). Cold-start conditions may have a significant impact on THC and NMHC emissions for fuels with high aromatics. Aromatic hydrocarbons have slower vaporization rates than paraffins, olefins, and alcohols,

resulting in higher concentrations of heavier aromatics in E10HA that will affect fuel volatility (i.e., T80 and T90 values). This will cause incomplete evaporation during cold-start conditions, leading to increased fuel impingement and higher formation of unburnt in-cylinder hydrocarbon emissions. CO emissions also increased 4.7 times during cold-start for E10HA relative to E10 fuel, similar to previous findings of PFI and GDI vehicles (Yang et al., 2019a; Zhu et al. 2017; Karavalakis et al., 2015). The higher aromatic content of the E10HA fuel led to ~50% higher NOx emissions during cold-start, although previous studies have reported mixed results with mostly not statistically significant differences (Karavalakis et al., 2015; Yang et al., 2019a; Yang et al., 2019c).

For the LA92 cycle, the use of E78 resulted in factors of 4.2-5.7 increase in THC, NMHC, and CO emissions relative to E10 during the cold-phase. Previous works have also demonstrated higher THC and CO emissions with higher ethanol blends (Karavalakis et al., 2012; Costagliola et al., 2013; Suarez-Bertoa et al., 2015a; Iodice et al., 2016; Timonen et al., 2017). It is theorized that the higher heat of vaporization of E78 possibly led to cooler conditions in the combustion chamber and suppressed fuel evaporation. During cold-start conditions, more liquid fuel will likely be trapped in the crevice, which would enhance THC emissions. Additionally, NO_x emissions increased significantly (factor of 6.8) for the cold-phase of LA92 on E78 compared to E10. Higher NOx emissions with increasing ethanol content were also seen in previous studies of older PFI vehicles (Durbin et al., 2007; Karavalakis et al., 2012; Costagliola et al., 2013).

The US06 cycle showed different trends than the LA92 cycle, exhibiting slight (<1% for NMHC) to moderate (~15% for THC and CO and 27% for NO_x) decreases in these emissions with E10HA compared to E10 (Table 2). The impact of higher ethanol content was particularly pronounced. Emissions of THC, NMHC, and CO decreased by 95%, 87%, and 33%, respectively,

with E78 compared to E10. The reductions in THC, NMHC, and CO emissions were primarily due to oxygen content of ethanol, which contributed to more oxygen in locally fuel-rich regions and to more complete combustion (Catapano et al., 2016; Yang et al., 2019c). NOx emissions showed some increase (30%) with E78 compared to E10 fuel, similar to LA92 cycle.

While no comparisons can be made between the PM mass and BC emissions for the E10 fuel over the LA92 cycle, weighted PM mass and BC emission factors were reduced by 57% and 66%, respectively, for E78 compared to E10HA (Table 1). For the LA92, total and solid particle number emissions for E78 showed large reductions of 54% and 64% compared to E10, and reductions of 91% and 76% compared to E10HA, respectively. The E10HA fuel showed more than a factor of 5 and 1.5 higher total and solid particle number emissions, respectively, relative to E10. The ratios of total particle number to solid particle number emissions were also increased for E10HA (7.89 for cold-start and 4.84 for weighted) compared to E10 (1.26 for cold-start and 1.38 for weighted) and E78 (2.25 for cold-start and 1.76 for weighted). The results reported here for the LA92 agree with other works demonstrating PM and particle number emissions reductions with higher ethanol blends (Yang et al., 2019c; Karavalakis et al., 2014a; Maricq et al., 2012; Jin et al., 2017). These reductions can be attributed to the higher oxygen content in the fuel, resulting in higher soot oxidation rates by the induction of HO_2 and OH free radicals, and the aromatics dilution hindering the formation of soot precursors during combustion and lowering the rates of soot surface growth via the hydrogen abstraction acetylene addition (HACA) mechanism (Khosousi et al., 2015; Lemaire et al., 2010; Yang et al., 2019c).

For the US06, particulate emissions were higher than the LA92 as a result of the more aggressive nature and the higher speeds and accelerations of the US06 cycle, which likely caused inefficient fuel vaporization and diffusive combustion during these driving conditions (Table 2).

For the US06 cycle, slight changes in BC emission factors (-3% to +13%) were observed for E78 compared to E10HA and E10 fuels, while total PM mass was increased by factors of 1.9-2.2 in E78. In contrast to the PM mass, the use of E78 led to total and solid particle number emission reductions by 84% and 19%, respectively, compared to E10. These findings likely suggest that the higher combustion temperature E78 fuel (as denoted by the higher NOx emissions) led to higher exhaust temperatures (not measured in this study), which probably led to desorption of carbon material from the exhaust transfer system and the subsequent contamination of the PM filter. A recent study has demonstrated that some degree of desorption would occur during aggressive driving (and high exhaust temperatures) experienced in the US06 cycle (Yang et al., 2020).

Average number size distributions of the emitted particles for the LA92 and US06 cycles are depicted in Figure 2. For the LA92, all fuels showed a dominant accumulation mode with a less distinctive nucleation mode. Particle populations in the accumulation mode were higher for E10HA and substantially lower for E78, consistent with the PM mass for these fuels over the LA92. Particle size distribution for E10HA shifted towards larger diameter (~53 nm), while E10 and E78 peaked at around 34 nm and 30 nm, respectively. For the US06, particle size distributions were decisively bimodal, with E10 showing higher particle populations in the nucleation mode (~10 nm). Accumulation mode particles dominated the size distribution for E78, with sizes centered at 60 nm compared to 70 nm for E10, particle populations similar to those of E10. It should be noted that E78 particle sizing data over the US06 does not support the higher gravimetric PM mass for this fuel compared to E10, suggesting that other mechanisms may have played a role in PM mass emissions, including the possible desorption of contaminants in the CVS tunnel that were released during the high temperature conditions over US06.

3.2 Secondary and aged PM over the LA92 cycle

Figure 3 shows the transient aged PM, SOA, aerosol nitrate, NOx, and NMHC emissions over the LA92 cycle for E10, E10HA, and E78 fuels. Note that non-refractory composition data from mAMS are not available from E10 runs. Real-time primary PM emissions and sulfate and ammonium ions over the LA92 are shown in Figure SM2 in SM. For all fuels, aged PM were seen at least about two orders of magnitude higher than primary PM emissions during the entire duration of LA92 cycle. When focusing on details of the time-resolved data, it was seen that the cold-start and acceleration events had the strongest influence on aged PM formation. Both E10 fuels resulted in higher concentrations and 5.7-8.1 times higher emission factors of aged PM relative to E78, with E10HA showing more aged PM than E10 (Table SM3, SM). Thus, our findings are consistent with previous studies of high ethanol blends (Timonen et al., 2017; Roth et al., 2020b; Suarez-Bertoa et al., 2015; Gramsch et al., 2018), but show more clearly the crucial role of driving conditions in the emissions of secondary aerosol precursors. Analogous to primary emissions, the presence of the oxygen atom in ethanol and the dilution of aromatics were the main factors for the reduced SOA formation. Ethanol promotes the formation of oxygenated species, such as carboxylic, carbonyl, and low molecular-weight ester compounds, which can seldomly act as SOA precursors. For example, this observation is supported by the results of a recent study that showed an abundance of alcohol, aldehydes, ketones, and ester compounds in primary aerosol from the exhaust of a GDI vehicle operated with E20 fuel over the LA92 cycle prior to irradiation in an environmental chamber (Roth et al., 2020a).

SOA formation was significantly affected by the cold-start period of the LA92 cycle, especially for E10HA fuel, which exhibited about 30 times more SOA mass during the first 200 seconds compared to the second large spike for this fuel at around 400 seconds. The cold-start emission

factor of SOA with E10HA was higher than E78 by factor of 11, as shown in Table SM3, SM. Our results agree with previous studies reporting on the dominance of the cold-start period on SOA formation from gasoline vehicles (Kuittinen et al., 2021; Karjalainen et al., 2016; Simonen et al., 2019; Pieber et al., 2018; Zhao et al., 2018; Saliba et al., 2017; Roth et al., 2020b). The substantially higher SOA mass for E10HA during cold-start was largely due to the presence of heavier aromatics for this fuel, which likely generated more IVOCs and SVOCs. Previous studies have proposed that IVOC emissions are important SOA precursors from gasoline vehicles (Robinson et al., 2007; Gentner et al., 2017; Drozd et al., 2019; Peng et al., 2017). McCaffery et al. (2020) showed that PFI FFVs when operated with alcohol fuels can be major contributors to aromatic IVOC emissions, with lower emission rates as alcohol content increased in gasoline. Aromatics are more difficult to evaporate during cold engine operation compared to other hydrocarbons, resulting in more liquid fuel wetting in the cylinder walls and increased formation of VOC precursors (Yang et al., 2019a). Roth et al. (2020b) demonstrated an important influence of heavier aromatics with high DBEs on SOA formation from a gasoline vehicle over the LA92 cycle. Drozd and co-workers (2019) reported that BTEX compounds contribute to about 40% of SOA formation from gasoline vehicles. Other studies have also shown the important contribution of BTEX species on SOA formation (Roth et al., 2020a; Nordin et al., 2013; Gordon et al., 2014; Timonen et al., 2017).

Overall, SOA formation was reduced significantly during the hot-running and hot-start phases of LA92 (by 2 orders of magnitude for E10HA and 4 orders of magnitude for E78), and coincided with the sharp acceleration events, as well as the tailpipe NMHC emissions. The higher SOA formation during cold-start was primarily attributed to the TWC being below its light-off temperature and therefore inefficient to oxidize SOA precursors (i.e., aromatic VOCs and other

NMHCs), leading to their higher emissions. In addition, the inefficient TWC also contributed to the semivolatile fraction of nanoparticles, which can act as seeds for further reactions in the TSAR, resulting in enhanced SOA mass. For the hot-running and hot-start phases, the higher intake air temperature, fuel temperature, and piston surface temperature aided improved fuel vaporization and resulted in lower SOA precursors emissions, which were also more efficiently oxidized in the TWC. Detailed composition of SOA (Figure 4) shows higher contribution from non-oxygenated $C_xH_y^+$ and intermediately oxygenated $C_xH_yO^+$ family of ions to OA compared to highly oxygenated $C_xH_yO_{z>1}^+$ (38-45% vs. 13-15%) during the cold-start phase of both E78 and E10HA while during the hot-running and hot-start phases, the contribution of $C_xH_yO_{z>1}^+$ was more comparable to or even higher than those of the less oxygenated fragments (Figure 4). During the cold-start phase, the contribution of each family of ions to OA was not significantly different between E78 and E10HA, suggesting that given the oxidation extent of the exhaust, similar types of OA functional groups were present in the SOA regardless of the fuel type. However, in the hot-running and hot-start phases, contribution of the intermediately oxygenated family ($C_xH_yO^+$) was significantly lower with E78 compared to E10HA.

Consistent with previous studies, inorganic secondary aerosol in the form of ammonium nitrate was found in elevated levels (Kuittinen et al., 2021; Vu et al., 2019; Roth et al., 2020a; Roth et al., 2020b; Gordon et al., 2014; Link et al., 2017). Total weighted emission factor of NO_3 was higher for E10HA compared to E78 (1.62 mg/mile vs. 0.47 mg/mile) (Table SM3, SM). The much lower NO_3 emission factor observed for E78 is counterintuitive since higher NOx emissions were observed for E78, especially during the cold-start phase. One possible explanation may be the lower OH exposure during the cold-start and subsequently lower nitric acid production during E78 runs; however, we do not have an estimate of the OH exposure during the LA92 run with E10HA.

Aerosol sulfate was found in much lower concentrations than nitrate and ammonium and was associated with cold-start and vehicle accelerations (Table SM3, SM). For E78, it comprised <0.2% of total secondary aerosol, as a consequence of the very low sulfur levels in the test fuels, while with E10HA, its contribution increased to 1.1% during the cold-start. Sulfate emission factor during the cold-start phase of LA92 on E10HA was 65 times higher than with E78. Furthermore, its total weighted emission factor was 20 times higher with E10HA compared to E78.

3.3 Secondary and aged PM over the US06 cycle

Figure 5 shows the transient aged PM, SOA, aerosol nitrate, NOx, and NMHC emissions over the US06 cycle for E10, E10HA, and E78 fuels. Real-time primary PM emissions and sulfate and ammonium ions over the US06 cycles are shown in Figure SM3, SM. Similar to LA92, for E10 fuel, aged PM were seen at least two orders of magnitude higher than primary PM emissions during the entire duration of the US06 cycle (comparison for E10HA fuel could not be carried out due to lack of EEPS measurements). Compared to both E10 fuels, aged PM emission factors for E78 were lower by 44-54%. When comparing the US06 and LA92, emission factors of aged PM compared differently with the weighted emission factors of aged PM during LA92 cycle depending on the fuel: emission factor of aged PM during US06 was comparable to that during LA92 on E10HA, 33% lower on E10, and a factor of 3.3 higher on E78. However, emission factors of aged PM on US06 were consistently lower than during the cold-start phase of LA92 for each fuel.

For the US06 cycle and similar to LA92, E10HA led to more SOA formation followed by E10 and E78. Consistently, measured OA relative to emitted CO was highest with E10HA and lowest with E78, as shown in Figure 6. Additionally, SOA emission factors on E10 were 50% lower than on E10HA and 3.5 times higher than on E78. Compared to LA92, SOA emission factors were 13-62% lower than the weighed SOA emission factors, with the largest difference observed for

E10HA. It is interesting to note that SOA formation was favored during acceleration events, with lower SOA during periods with steady high speed and no rapid accelerations (i.e., ~200-300 sec and ~350-480 sec). This was noticeable within the period of steady high-speed driving at ~300 seconds, where a rapid acceleration led to more NMHC emissions and SOA formation. The E10HA fuel contained higher levels of BTEX and heavier aromatics than E10. Aromatic VOC emissions were likely to occur during acceleration events and high-speed driving, which affected SOA production. This is due to the fact that higher boiling point aromatics will require longer time to evaporate, especially during the high speed and power conditions of the US06 when longer fuel injection duration is demanded, resulting in higher precursor emissions. Assuming the relative composition of the monoaromatics, naphthalenes, and naphtheno/olefin benzenes of the exhaust is similar to those in the fuels, we can compare the SOA formation potential of these compounds from using different fuels. In this exercise, contributions of other hydrocarbons from the fuel (namely, paraffins, napththenes, olefins, and oxygenates) are ignored since the weighted carbon number in each class was C2 to less than C8, making them on average too small in size and insignificant for SOA formation. By scaling the literature-based SOA yield values of various aromatic species (based on carbon number and compound class (Gentner et al., 2012)) with the corresponding carbon weight fraction in the fuel, we estimated the corresponding weighted cumulative SOA yield values for E78, E10, and E10HA to be 0.53, 2.96, and 3.87, respectively. The yield values are dominated by C7-C10 monoaromatic species (Table SM4, SM). Although these values do not necessarily reflect the actual SOA yield of the exhaust emissions, they support the observation that SOA formations from E10 and E10HA are significantly higher than from E78. In fact, because of the higher aromatic (C6-C12) content of E10HA, its cumulative SOA formation potential is estimated to be 30% and factor of 7.3 higher than that of E10 and E78, respectively,

assuming hydrocarbon emissions in the exhaust follow the same composition as the fuel itself (Table SM4, SM). To a first approximation, the differences between the observed emission factors of SOA for different fuels during US06 operation are consistent with this simple calculation: the emission factor on E10HA was 51% and factor of 5.3 higher than E10 and E78, respectively. Despite differences in the extent of SOA formation from these different fuels, and consistent with the observations from the LA92 runs, the overall composition of OA was similar between US06 runs with different fuels (Figure SM4, SM).

Similar to LA92, nitrate emission factors decreased in US06 in the following order: E10>E10HA>E78. However, for the US06, nitrate emission factors were higher than LA92 by factors of 1.5 and 3.3 for E10HA and E78, respectively, despite slightly lower overall OH exposures in US06 vs. LA92 runs on E78 (6.7 days vs. 7.0 days; OH exposure on E10HA for LA92 not available). This can be explained by the higher combustion temperature and the enhanced generation of NOx emissions during the more dynamic driving of US06 as seen by about twice as high NOx emissions on E10HA and E78 compared to LA92 (NOx emissions on US06 with E10 are not available), which favor secondary nitrate aerosol formation. For the E10 fuel, the emission factor of NO_3 was lower during US06 than LA92 by 33%. While nitrate aerosol was produced throughout the entire duration of US06, large nitrate spikes were only seen during the sharp accelerations of LA92 and during cold-start. For both cycles, nitrate aerosol was lower for E78, suggesting that the introduction of higher ethanol blends in the light-duty vehicle market will potentially result in nitrate aerosol reductions.

The use of E78 led to lower ammonium aerosol concentrations relative to both E10 fuels for both US06 and LA92 cycles, indicating beneficial ethanol effects on inorganic aerosol formation. Consistent with the trend for nitrate, ammonium aerosol concentrations were also higher for the

US06 compared to LA92 on E10HA (by 56%) and E78 (by factor of 5.3). Ammonium nitrate formation is usually favored by tailpipe ammonia (NH_3) emissions formed in the TWC from NO reduction by hydrogen produced from the water gas shift reaction of CO or via hydrocarbon steam reforming (Link et al., 2017; Suarez-Bertoa et al., 2015b). NH_3 emissions largely depend on rich-fuel conditions, typical of accelerations and dynamic driving where elevated CO concentrations also occur. Although NH_3 emissions were not measured in this study, CO emission factors correlated positively with that of ammonium for US06 (Figure SM5, SM). Similar findings were reported by Link et al. (2017) when they tested gasoline vehicles using an OFR. Our results suggest that ammonium nitrate production was primarily driven by NH_3 emissions rather than NOx emissions.

For the US06 cycle, aerosol sulfate mostly peaked during accelerations and high-speed driving conditions. Similar to LA92, the use of the lowest sulfur content E78 fuel led to lowest concentrations of sulfate. In fact, emission factor of aerosol sulfate during US06 using E78 was half of those of either E10 fuels. Sulfate is usually sourced from fuel and lubricant oil sulfur compounds stored in the TWC and eventually released as SO_2 prompting the formation of sulfate aerosol, especially during accelerations and high-speed conditions (Simonen et al., 2019; Karjalainen et al., 2014). Thus, it is expected that more aerosol sulfate is generated during cold-starts due to the partially evaporated fuel and lubricant oil components, and dynamic driving conditions due to the higher fuel and lubricant oil consumption. This explains why sulfate emission factors on E10HA were significantly (~80 times) higher during the cold-start phase of LA92 versus US06, whereas the emission factor for the cold-start of LA92 on E10 was only 77% higher than US06 on E10.

4. Conclusions

This study examined the primary emissions and secondary aerosol formation potential from an FFV equipped with a PFI gasoline engine when operated with two E10 fuels of different aromatic contents and an E78 blend. Testing was conducted over the LA92 and US06 driving cycles using a chassis dynamometer. Primary emission results showed mixed trends across the different fuels and driving cycles. The use of E78 led to increases in THC, NMHC, CO, NOx emissions over the LA92 compared to E10 fuels, but decreases in these pollutants over the US06. Particulate emissions, including PM mass, BC, total and solid particle number showed reductions with E78 compared to E10 fuels for both cycles. An exception was seen for the PM mass with E78 over the US06, which is believed to have been caused by the contamination of the exhaust transfer system during aggressive driving and high exhaust temperature conditions.

Secondary aerosol formation potential measured with an oxidation flow reactor was strongly dependent on cold-start conditions and especially during the first 200-300 seconds of the cycle. Strong influence on the formation of secondary aerosol was also seen during the sharp acceleration events of the LA92 and US06 cycles. The higher aromatics E10 fuel produced greater concentrations of secondary aerosol compared to E10, whereas the E78 blend resulted in the least secondary aerosol formation. Ammonium nitrate formation was elevated for both test cycles and fuels, with the E78 blend leading to lower inorganic aerosol formation. Overall, this study showed the beneficial effects on secondary aerosol forming potential by using high ethanol blends in gasoline vehicles and the adverse effects of high aromatic content fuels on primary emissions and secondary aerosol formation. The results reported here also revealed that during cold-start operation fuel composition will likely play a key role on secondary aerosol production due to the higher generation of secondary aerosol precursors at the tailpipe, and highlighted the importance

of using transient conditions and time-resolved characterization in research focusing on secondary aerosols linked with mobile sources.

Acknowledgements

The authors thank the late Mr. Kurt Bumiller for helping setting up the experiment and dedicate this publication to his memory. We thank Mr. Mark Villela and Mr. Daniel Gomez of the University of California, Riverside for their contribution in conducting testing for this research program. We acknowledge funding from CARTEEH (Center for Advancing Research in Transportation Emissions, Energy, and Health), a US Department of Transportation's University Transportation Center, and USDA-NIFA Hatch (Project No. CA-R-ENS-5072-H, Accession No. 1015963). Niina Kuittinen acknowledges funding from Tampere University Graduate School and the American-Scandinavian Foundation. Niina Kuittinen and Topi Rönkkö acknowledges funding for the Black Carbon Footprint project, granted by Business Finland, Finnish authorities and companies.

References

Aikawa, K., Sakurai, T., Jetter, J. J. Development of a predictive model for gasoline vehicle particulate matter emissions. SAE Int. J. Fuels Lubr. 2010, 3, 610-622.

Bahreini, R., Middlebrook, A. M., de Gouw, J. A., Warneke, C., Trainer, M., Brock, C. A., Stark, H., Brown, S. S., Dube, W. P., Gilman, J. B., Hall, K., Holloway, J. S., Kuster, W. C., Perring, A. E., Prevot, A. S. H., Schwarz, J. P., Spackman, J. R., Szidat, S., Wagner, N. L., Weber, R. J., Zotter, P., Parrish, D. D. Gasoline emissions dominate over diesel in formation of secondary organic aerosol mass. Geophys. Res. Lett. 2012a, 39, L06805, doi: 10.1029/2011GL050718.

Bahreini, R., Middlebrook, A. M., Brock, C. A., de Gouw, J. A., McKeen, S. A., Williams, L. R., Daumit, K. E., Lambe, A. T., Massoli, P., Canagaratna, M. R., Ahmadov, R., Carrasquillo, A. J.; Cross, E. S., Ervens, B., Holloway, J. S., Hunter, J. F.; Onasch, T. B., Pollack, I. B., Roberts, J. M.; Ryerson, T. B., Warneke, C., Davidovits, P., Worsnop, D. R., Kroll, J. H. Mass spectral analysis of organic aerosol formed downwind of the deepwater horizon oil spill: Field studies and laboratory confirmations. Environ. Sci. Technol. 2012b, 46, 8025-8034

Cao, J., Wang, Q., Li, L., Zhang, Y., Tian, J., Antony Chen, L.W., Hang-Ho, S.S., Wang, X., Chow, J.C., Watson, J.G. Evaluation of the oxidation flow reactor for particulate matter emission limit certification. Atmospheric Environment 2020, 224, 117086.

Catapano, F., Sementa, P., Vaglieco, B.M. Air-fuel mixing and combustion behaviour of gasoline-ethanol blends in a GDI wall-guided turbocharged multi-cylinder optical engine. Renewable Energy 2016, 96, 319-332.

Clairotte, M., Adam, T.W., Zardini, A.A., Manfredi, U., Martini, G., Krasenbrink, A., Vicet, A., Tournie, E., Astorga, C. Effects of low temperature on the cold start gaseous emissions from light duty vehicles fueled by ethanol-blended gasoline. Applied Energy 2013, 102, 44-54.

Collier, S.; Zhang, Q. Gas-phase CO2 subtraction for improved measurements of the organic aerosol mass concentration and oxidation degree by an aerosol mass spectrometer. Environ. Sci. Technol. 2013, 47, 14324–14331.

Costagliola, M.A., De Simio, L., Pratti, M.V. Combustion efficiency and engine out emissions of a S.I. engine fueled with alcohol/gasoline blends. Applied Energy 2013, 111, 1162-1171.

Derwent, R.G., Jenkin, M.E., Utembe, S.R., Shallcross, D.E., Murrells, T.P., Passant, N.R. Secondary Organic Aerosol Formation from a Large Number of Reactive Man-Made Organic Compounds. Science of the Total Environment 2010, 408, 3374-3381.

Drozd, G.T., Zhao, Y., Saliba, G., Frodin, B., Maddox C., Chang, M.C.O., Maldonado, H., Sardar, S., Weber, R.J., Robinson, A.L., Goldstein, A.H. Detailed speciation of intermediate volatility and semivolatile organic compound emissions from gasoline vehicles: Effects of cold-starts and implications for secondary organic aerosol formation. Environ. Sci. Technol. 2019, 53, 1706-1714.

Du, Z., Hu, M., Peng, J., Zhang, W., Zheng, J., Gu, F., Qin, Y., Yang, Y., Li, M., Wu, Y., Shao, M., Shuai, S. Comparison of primary aerosol emission and secondary aerosol formation from gasoline direct injection and port fuel injection vehicles. Atmos. Chem. Phys. 2018, 18, 9011-9023.

Durbin, T.D., Miller, J.W., Younglove, T., Huai, T., Cocker, K. Effects of Fuel Ethanol Content and Volatility on Regulated and Unregulated Exhaust Emissions for the Latest Technology Gasoline Vehicles. Environ. Sci. Technol. 2007, 41, 4059-4064.

Fushimi, A., Kondo, Y., Kobayashi, S., Fujitani, Y., Saitoh, K., Takami, A., Tanabe, K. Chemical composition and source of fine and nanoparticles from recent direct injection gasoline passenger cars: Effects of fuel and ambient temperature. Atmospheric Environment 2016, 124, 77-84.

Gentner, D.R., Isaacman, G., Worton, D.R., Chan, A.W.H., Dallmann, T.R., Davis, L., Liu, S., Day, D.A., Russell, L.M., Wilson, K.R., Weber, R., Guha, A., Harley, R.A., Goldstein, A.H. Elucidating secondary organic aerosol from diesel and gasoline vehicles through detailed characterization of organic carbon emissions. Proceedings of the National Academy of Sciences of the United States of America 2012, 109, 18318-18323.

Gentner, D.R., Jathar, S.H., Gordon, T.D., Bahreini, R., Day, D.A., Haddad, I.E., Haynes, P.L., Pieber, S.M., Platt, S.M., De Gouw, J., Goldstein, A.H., Harley, R.A., Jimenez, J.L., Prevot,

A.S.H., Robinson A.L. Review of urban secondary organic aerosol formation from gasoline and diesel motor vehicle emissions. Environ. Sci. Technol. 2017, 51, 1074-1093.

Gordon, T. D., Presto, A. A., May, A. A., Nguyen, N. T., Lipsky, E. M., Donahue, N. M., Gutierrez, A., Zhang, M., Maddox, C., Rieger, P., Chattopadhyay, S., Maldonado, H., Maricq, M. M., Robinson, A. L. Secondary organic aerosol formation exceeds primary particulate matter emissions for light-duty gasoline vehicles. Atmos. Chem. Phys. 2014, 14, 4661–4678.

Gramsch, E., Papapostolou, V., Reyes, F., Vásquez, Y., Castillo, M., Oyola, P., López, G., Cadiz, A., Ferguson, S., Wolfson, M., Lawrence, J., Koutrakis, P. Variability in the Primary Emissions and Secondary Gas and Particle Formation from Vehicles Using Bioethanol Mixtures. Journal of the Air & Waste Management Association 2018, 68, 329-46.

Hays, M.D., Preston, W., George, B.J., Schmid, J., Baldauf, R., Snow, R., Robinson, J.R., Long, T., Faircloth, J. Carbonaceous aerosols emitted from light-duty vehicles operating on gasoline and ethanol fuel blends. Environ. Sci. Technol. 2013, 47, 14502-14509.

He, Y., King, B., Pothier, M., Lewane, L., Akherati, A., Mattila, J., Farmer, D.K., McCormick, R.L., Thornton, M., Pierce, J.R., Volckens, J., Jathar, S.H. Secondary organic aerosol formation from evaporated biofuels: comparison to gasoline and correction for vapor wall losses. Environ. Sci.: Processes Impacts 2020, 22, 1461-1474.

Iodice, P., Senatore, A., Langella, G., Amoresano, A. Effect of ethanol-gasoline blends on CO and HC emissions in last generation SI engines within the cold-start transient: An experimental investigation. Applied Energy 2016, 179, 182-190.

Jathar, S.H., Miracolo, M.A., Tkacik, D.S., Donahue, N.M., Adams, P.J., Robinson, A.L. Secondary organic aerosol formation from photo-oxidation of unburned fuel: Experimental

results and implications for aerosol formation from combustion emissions. Environ. Sci. Technol. 2013, 47, 12886-12893.

Jayne, J. T., Leard, D. C., Zhang, X., Davidovits, P., Smith, K. A., Kolb, C. E., Worsnop, D. W. Development of an Aerosol Mass Spectrometer for size and composition analysis of submicron particles. Aerosol Sci. Technol. 2000, 33, 49-70.

Jimenez, J. L., Canagaratna, M. R., Donahue, N. M., Prevôt, A. S. H., Zhang, Q., Kroll, J. H., Decarlo, P. F., Allan, J. D., Coe, H., Ng, N. L., Aiken, A. C., Ulbrich, I. M., Grieshop, A. P., Duplissy, J., Wilson, K. R., Lanz, V. A., Hueglin, C., Sun, Y. L., Tian, J., Laaksonen, A., Raatikainen, T., Rautiainen, J., Vaattovaara, P., Ehn, M., Kulmala, M., Tomlinson, J. M., Cubison, M. J., Dunlea, E. J., Alfarra, M. R., Williams, P. I., Bower, K., Kondo, Y., Schneider, J., Drewnick, F., Borrmann, S., Weimer, S., Demerjian, K., Salcedo, D., Cottrell, L., Takami, A., Miyoshi, T., Shimono, A., Sun, J. Y., Zhang, Y. M., Dzepina, K., Sueper, D., Jayne, J. T., Herndon, S. C., Williams, L. R., Wood, E. C., Middlebrook, A. M., Kolb, C. E., Baltensperger, U., Worsnop, D. R. Evolution of organic aerosols in the atmosphere. Science 2009, 326, 1525–1529.

Jin, D., Cho, K., Myun, C.L., Lim, Y., Lee, J., Park, S. The impact of various ethanol-gasoline blends on particulates and unregulated gaseous emissions characteristics from a spark ignition direct injection (SIDI) passenger vehicle. Fuel 2017, 209, 702-712.

Kanakidou, M., Seinfeld, J.H., Pandis, S.N., Barnes, I., Dentener, F.J., Facchini, M.C., Van Dingenen, R., Ervens, B., Nenes, A., Nielsen, C.J., Swietlicki, E., Putaud, J.P., Balkanski, Y., Fuzzi, S., Horth, J., Moortgat, G.K., Winterhalter, R., Myhre, C.E.L., Tsigaridis, K., Vignati, E., Stephanou, E.G., Wilson, J. Organic aerosol and global climate modelling: a review. Atmos. Chem. Phys. 2005, 5, 1053-1123.

Kang, E., Root, M., Toohey, D.W., Brune, W.H. Introducing the concept of Potential Aerosol Mass (PAM). Atmos. Chem. Phys. 2007, 7, 5727-5744.

Karavalakis, G., Durbin, T.D., Shrivastava, M., Zheng, Z., Villela, M., Jung, H. Impacts of ethanol fuel level on emissions of regulated and unregulated pollutants from a fleet of gasoline light-duty vehicles. Fuel 2012, 93, 549-558.

Karavalakis, G., Short, D., Vu, D., Villela, M., Asa-Awuku, A., Durbin, T.D. Evaluating the regulated emissions, air toxics, ultrafine particles, and black carbon from SI-PFI and SI-DI vehicles operating on different ethanol and iso-butanol blends. Fuel 2014a, 128, 410-421.

Karavalakis, G., Short, D., Russell, R.L., Jung, H., Johnson, K.C., Asa-Awuku, A., Durbin, T.D. Assessing the Impacts of Ethanol and Iso-butanol on Gaseous and Particulate Emissions from Flexible Fuel Vehicles. Environ. Sci. Technol. 2014b, 48, 14016-14024.

Karjalainen, P., Prjola, L., Heikkila, J., Lahde, T., Tzamkiozis, T., Ntziachristos, L., Keskinen, J., Ronkko, T. Exhaust particles of modern gasoline vehicles: A laboratory and an on-road study. Atmospheric Environment 2014, 97, 262-270.

Karjalainen, P., Timonen, H., Saukko, E., Kuuluvainen, H., Saarikoski, S., Aakko-Saksa, P., Murtonen, T., Dal Maso, M., Ahlberg, E., Svenningsson, B., Brune, W. H., Hillamo, R., Keskinen, J., Rönkkö, T. Time-resolved characterization of primary and secondary particle emissions of a modern gasoline passenger car. Atmos. Chem. Phys. 2016, 16, 8559–8470.

Khosousi, A., Liu, F., Dworkin, S.B., Eaves, N.A., Thomson, M.J., He, X., Dai, Y., Gao, Y., Liu, F., Shuai, S., Wang, J. Experimental and numerical study of soot formation in laminar coflow diffusion flames off gasoline/ethanol blends. Combustion and Flame 2015, 162, 3925-3933.

Kuittinen, N., McCaffery, C., Peng, W., Zimmerman, S., Roth, P., Simonen, P., Karjalainen, P., Keskinen, J., Cocker, D.R., Durbin, T.D., Ronkko, T., Bahreini, R., Karavalakis, G. Effects of

driving conditions on secondary aerosol formation from a GDI vehicle using an oxidation flow reactor. Environmental Pollution 2021, 282, 117069.

Lambe, A.T., Ahern, J.P.D., Brune, W.H., Ng, N.L., Wright, J.P., Croasdale, D.R., Worsnop, D.R., Davidovits, P., Onasch, T.B. Characterization of aerosol photooxidation flow reactors heterogeneous oxidation, secondary organic aerosol formation and cloud condensation nuclei activity measurements. Atmos. Meas. Tech. 2011, 4, 445-461.

Lemaire, R., Therssen, E., Desgroux, P. Effect of ethanol addition in gasoline and gasoline-surrogate on soot formation in turbulent spray flames. Fuel 2010, 89, 3952-3959.

Link, M.F., Kim, J., Park, G., Lee, T., Park, T., Babar, Z.B., Sung, K., Kang, S., Kim, J.S., Choi, Y., Son, J., Lim, H.-J., Farmer, D.K. Elevated production of NH4NO3 from the photochemical processing of vehicle exhaust: Implications for air quality in the Seoul Metropolitan Region. Atmospheric Environment 2017, 156, 95-101.

Maricq, M.M., Szente, J.J., Jahr, K. The impact of ethanol fuel blends on PM emissions from a light-duty GDI vehicle. Aerosol Science and Technology 2012, 46, 576-583.

McCaferry, C., Durbin, T.D., Johnson, K.C., Karavalakis, G. The effect of ethanol and iso-butanol blends on polycyclic aromatic hydrocarbon (PAH) emissions from PFI and GDI vehicles.

Ng, N. L., Canagaratna, M. R., Jimenez, J. L., Zhang, Q., Ulbrich, I. M., Worsnop, D. R. Real-time methods for estimating organic component mass concentrations from aerosol mass spectrometer data. Environ. Sci. Technol. 2011, 45, 910-916.

Nordin, E. Z., Eriksson, A. C., Roldin, P., Nilsson, P. T., Carlsson, J. E., Kajos, M. K., Hellén, H., Wittbom, C., Rissler, J., Löndahl, J., Swietlicki, E., Svenningsson, B., Bohgard, M., Kulmala, M., Hallquist, M., Pagels, J. H. Secondary organic aerosol formation from idling gasoline

passenger vehicle emissions investigated in a smog chamber. Atmos. Chem. Phys. 2013, 13, 6101-6116.

Middlebrook, A. M.; Bahreini, R.; Jimenez, J. L.; Canagaratna, M. R. Evaluation of composition-dependent collection efficiencies for the Aerodyne aerosol mass spectrometer using field data. Aerosol Science and Technology 2012, 46, 258-271.

Ortega, A. M., Hayes, P. L., Peng, Z., Palm, B. B., Hu, W., Day, D. A., Li, R., Cubison, M. J., Brune, W. H., Graus, M., Warneke, C., Gilman, J. B., Kuster, W. C., de Gouw, J., Gutiérrez-Montes, C., Jimenez, J. L. Real-time measurements of secondary organic aerosol formation and aging from ambient air in an oxidation flow reactor in the Los Angeles area, Atmos. Chem. Phys. 2016, 16, 7411–7433.

Peng, J., Hu, M., Du, Z., Wang, Y., Zheng, J., Zhang, W., Yang, Y., Qin, Y., Zheng, R., Xiao, Y., Wu, Y., Lu, S., Wu, Z., Guo, S., Mao, H., Shuai, S. Gasoline aromatics: a critical determinant of urban secondary organic aerosol formation. Atmos. Chem. Phys. 2017, 17, 10743-10752.

Pieber, S. M., Kumar, N. K., Klein, F., Comte, P., Bhattu, D., Dommen, J., Bruns, E. A., Kilic, D., El Haddad, I., Keller, A., Czerwinski, J., Heeb, N., Baltensperger, U., Slowik, J. G., Prévôt, A. S. H. Gas-phase composition and secondary organic aerosol formation from standard and particle filter-retrofitted gasoline direct injection vehicles investigated in a batch and flow reactor. Atmos. Chem. Phys. 2018, 18, 9929-9954.

Platt, S.M., El Haddad, I., Pieber, S.M., Zardini, A.A., Suarez-Bertoa, R., Clairotte, M., Daellenbach, K.R., Huang, R.-J., Slowik, J.G., Hellebust, S., Temime-Roussel, B., Marchand, N., de Gouw, J., Jimenez, J.L., Hayes, P.L., Robinson, A.L., Baltensperger, U., Astorga, C., Prévôt, A.S.H. Gasoline cars produce more carbonaceous particulate matter than modern filter-

equipped diesel cars. Scientific Reports 2017, 7, 4926, https://doi.org/10.1038/s41598-017-03714-9.

Robinson, A. L., Donahue, N. M., Shrivastava, M. K., Weitkamp, E.A., Sage, A. M., Grieshop, A.P., Lane, T. E., Pierce, J. R., Pandis, S. N. Rethinking Organic Aerosols: Semivolatile Emissions and Photochemical Aging. Science 2007, 315, 1259–1262.

Roth, P., Yang, J., Fofie, E., Cocker, D. R., Durbin, T. D., Brezny, R., Geller, M., Asa-Awuku, A., Karavalakis, G. Catalyzed gasoline particulate filters reduce secondary organic aerosol production from gasoline direct injection vehicles. Environ. Sci. Technol. 2019, 53, 3037-3047.

Roth, P.; Yang, J.; Stamatis, C.; Barsanti, K.C.; Cocker, III D.R.; Durbin, T.D.; Asa-Awuku, A.; Karavalakis, G. Evaluating the relationships between aromatic and ethanol levels in gasoline on secondary aerosol formation from a gasoline direct injection vehicle. Science of the Total Environment 2020a, 737, 140333.

Roth, P., Yang, J., Peng, W., Cocker III, D.R., Durbin, T.D., Asa-Awuku, A., Karavalakis G. Intermediate and high ethanol blends reduce secondary organic aerosol formation from gasoline direct injection vehicles. Atmospheric Environment 2020b, 220, 117064.

Saliba, G.; Saleh, R.; Zhao, Y.; Presto, A.A.; Lamber, A.T.; Frodin, B.; Sardar, S.; Maldonado, H.; Maddox, C.; May, A.A.; Drozd, G.T.; Goldstein, A.H.; Russell, L.M.; Hagen,, F.; Robinson, A.L. Comparison of gasoline direct-injection (GDI) and port fuel injection (PFI) vehicle emissions: Emission Certification standards, cold-start, secondary organic aerosol formation potential, and potential climate impacts. Environ. Sci. Technol. 2017, 51, 6542-6552.

Simonen, P.; Saukko, E.; Karjalainen, P.; Timonen, H.; Bloss, M.; Aakko-Saksa, P.; Rönkkö, T.; Keskinen, J.; Dal Maso, M. A new oxidation flow reactor for measuring secondary aerosol formation of rapidly changing emission sources. Atmos. Meas. Tech. 2017, 10, 1519-1537.

Simonen P., Kalliokoski J., Karjalainen P., Ronkko T., Timonen H., Saarikoski S., Aurela M., Bloss M, Triantafyllopoulos G., Kontses A., Amanatidis S., Dimaratos A., Samaras Z., Keskinen J., Dal Maso M., Ntziachristos L. Characterization of laboratory and real driving emissions of individual Euro 6 light-duty vehicles – Fresh particles and secondary aerosol formation. Environmental Pollution 2019, 255, 113175.

Suarez-Bertoa, R., Zardini, A.A., Keuken, H., Astorga, C. Impact of ethanol containing gasoline blends on emissions from a flex-fuel vehicle tested over the Worldwide Harmonized Light duty Test Cycle (WLTC). Fuel 2015a, 143, 173-182.

Suarez-Bertoa, R., Zardini, A.A., Platt, S.M., Hellebust, S., Pieber, S.M., Haddad, I.E., Temime-Roussel, B., Baltensperger, U., Marchand, N., Prevot, A.S.H., Astorga, C. Primary emissions and secondary organic aerosol formation from the exhaust of a flex-fuel (ethanol) vehicle. Atmospheric Environment 2015b, 177, 200-211.

Timonen, H., Karjalainen, P., Saukko, E., Saarikoski, S., Aakko-Saksa, P., Simonen, P., Murtonen, T., Maso, M.D., Kuuluvainen, H., Bloss, M., Ahlberg, E., Svenningsson, B., Pagels, J., Brune, W.H., Keskinen, J., Worsnop, D.R., Hillamo, R., Ronkko, T. Influence of Fuel Ethanol Content on Primary Emissions and Secondary Aerosol Formation Potential for a Modern Flex-Fuel Gasoline Vehicle. Atmos. Chem. Phys. 2017, 17, 5311–5329.

Tkacik, D.S., Lambe, A. T., Jathar, S., Li, X., Presto A.A., Zhao, Y., Blake, D., Meinardi, S., Jayne, J. T., Croteau, P. L., Robinson, A. L. Secondary organic aerosol formation from in-use

motor vehicle emissions using a potential aerosol mass reactor. Environ. Sci. Technol. 2014, 48, 11235-11242.

Tuet, W.Y., Chen, Y., Fok, S., Champion, J.A., Ng, N.L. Inflammatory responses to secondary organic aerosols (SOA) generated from biogenic and anthropogenic precursors. Atmos. Chem. Phys. 2017, 17, 11423-11440.

Vu, D., Roth, P., Berte, T., Yang, J., Cocker, D.R., Durbin, T., Karavalakis, G., Asa-Awuku, A. Using a new Mobile Atmospheric Chamber (MACh) to investigate the formation of secondary aerosols from mobile sources: The case of gasoline direct injection vehicles. Journal of Aerosol Science 2019, 133, 1-11.

Vu, K. T.; Dingle, J. H.; Bahreini, R.; Reddy, P. J.; Apel, E. C.; Campos, T. L.; DiGangi, J. P.; Diskin, G. S.; Fried, A.; Herndon, S. C.; Hills, A. J.; Hornbrook, R. S.; Huey, G.; Kaser, L.; Montzka, D. D.; Nowak, J. B.; Pusede, S. E.; Richter, D.; Roscioli, J. R.; Sachse, G. W.; Shertz, S.; Stell, M.; Tanner, D.; Tyndall, G. S.; Walega, J.; Weibring, P.; Weinheimer, A. J.; Pfister, G.; Flocke, F. Impacts of the Denver Cyclone on regional air quality and aerosol formation in the Colorado Front Range during FRAPPÉ 2014. Atmos. Chem. Phys. 2016, 16, 12039-12058.

Yang, J., Roth, P., Durbin, T., Karavalakis, G. Impacts of gasoline aromatic and ethanol levels on the emissions from GDI vehicles: Part 1. Influence on regulated and gaseous toxic pollutants. Fuel 2019a, 252, 799-811.

Yang, J., Roth, P., Zhu, H., Durbin, T.D., Karavalakis, G. Impacts of gasoline aromatic and ethanol levels on the emissions from GDI vehicles: Part 2. Influence on particulate matter, black carbon, and nanoparticle emissions. Fuel 2019b, 252, 812-820.

Yang, J., Roth, P., Durbin, T.D., Johnson, K.C., Asa-Awuku, A., Cocker, III D.R., Karavalakis G. Investigation of the effect of mid- and high-level ethanol blends on the particulate and the

mobile source air toxic (MSAT) emissions from a GDI flex fuel vehicle. Energy and Fuels 2019c, 33, 429-440.

Yang. J., Pham, L., Johnson, K.C., Durbin, T.D., Karavalakis, G., Kittelson, D., Jung, H. Impacts of exhaust transfer system contamination on particulate matter measurements. Emission Control Science and Technology 2020, 6, 163-177.

Yao, C., Dou, Z., Wang, B., Liu, M., Lu, H., Feng, J., Feng, L. Experimental study of the effect of heavy aromatics on the characteristics of combustion and ultrafine particle in DISI engine. Fuel 2017, 203, 290-297.

Zhao, Y., Lamber, A.T., Saleh, R., Saliba, G., Robinson, A.L. Secondary organic aerosol production from gasoline vehicle exhaust: Effects of engine technology, cold start, and emission certification standard. Environ. Sci. Technol. 2018, 52, 1253-1261.

Zhu, R., Hu, J., Bao, X., He, L., Zu, L. Effects of aromatics, olefins and distillation temperatures (T50 & T90) on particle mass and number emissions from gasoline direct injection (GDI) vehicles. Energy Policy 2017, 101, 185-193.

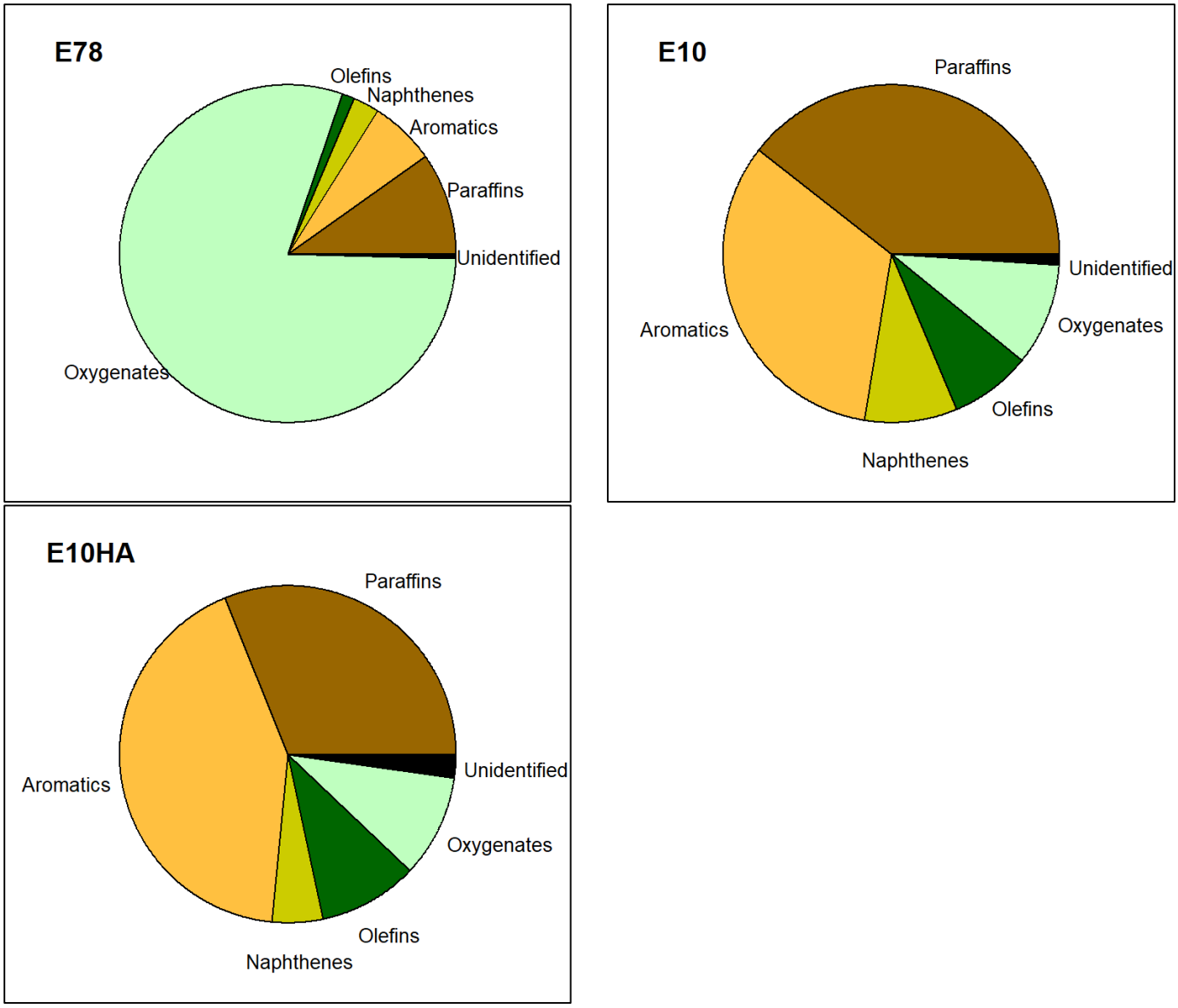

Figure 1: Fuel composition as a function of the major compound family

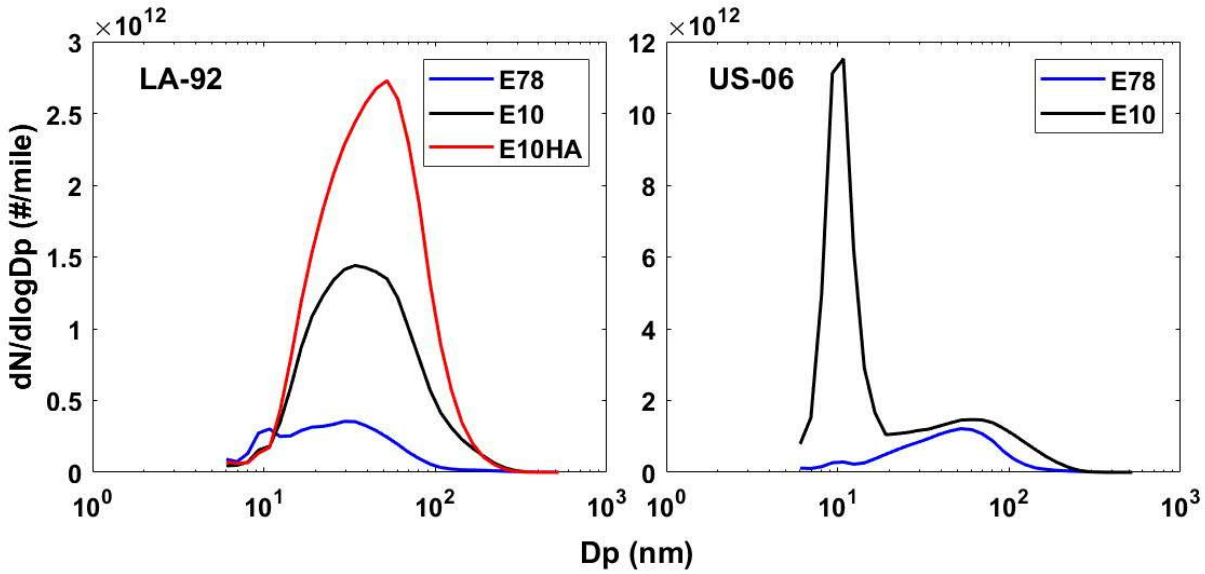

Figure 2: Average particle number size distributions over the LA92 (left-hand side) and US06 (right-hand side) cycles

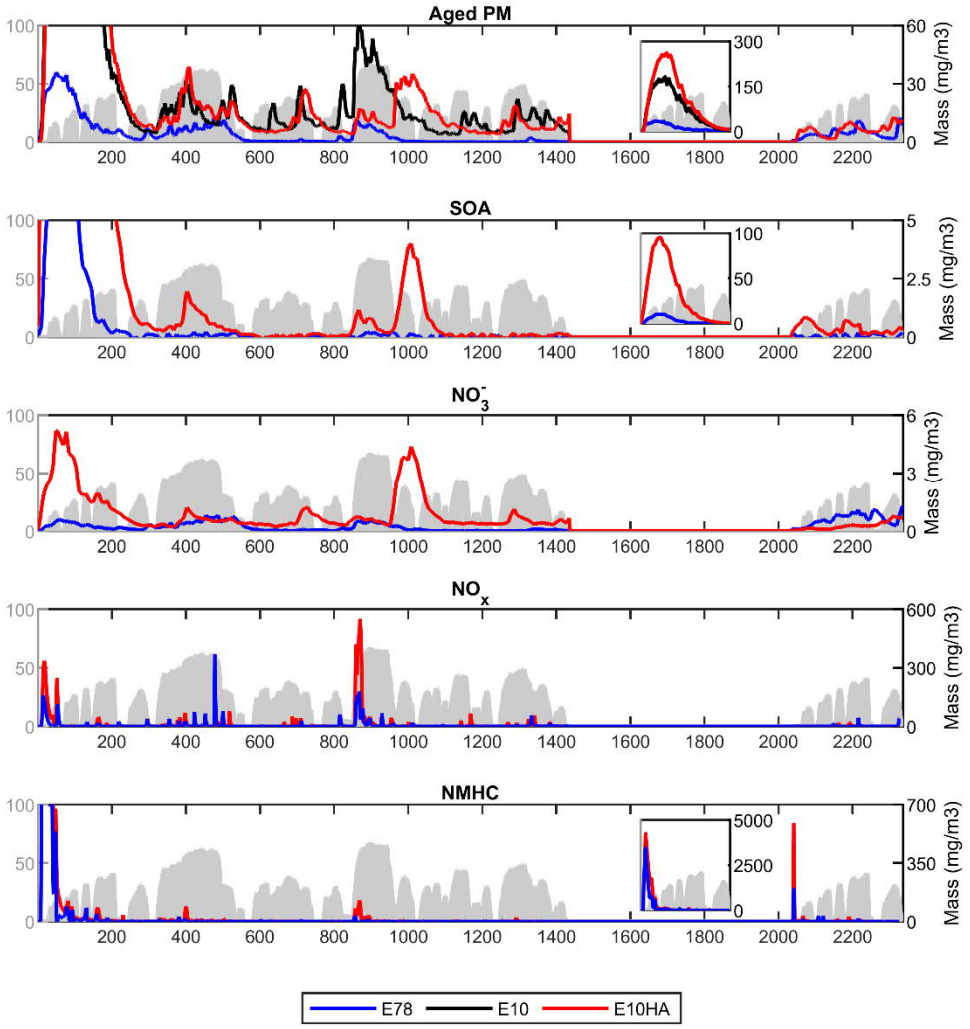

Figure 3: Aged PM, SOA, nitrate, NOx, and NMHC concentration over the LA92 cycle with E10, E10HA, and E78. For E10 fuel, only aged PM data is available over the cold-start and hot-running phases. Subfigures show the first 300 seconds of the cold-start phase. Shown concentrations have been corrected to represent tailpipe concentrations.

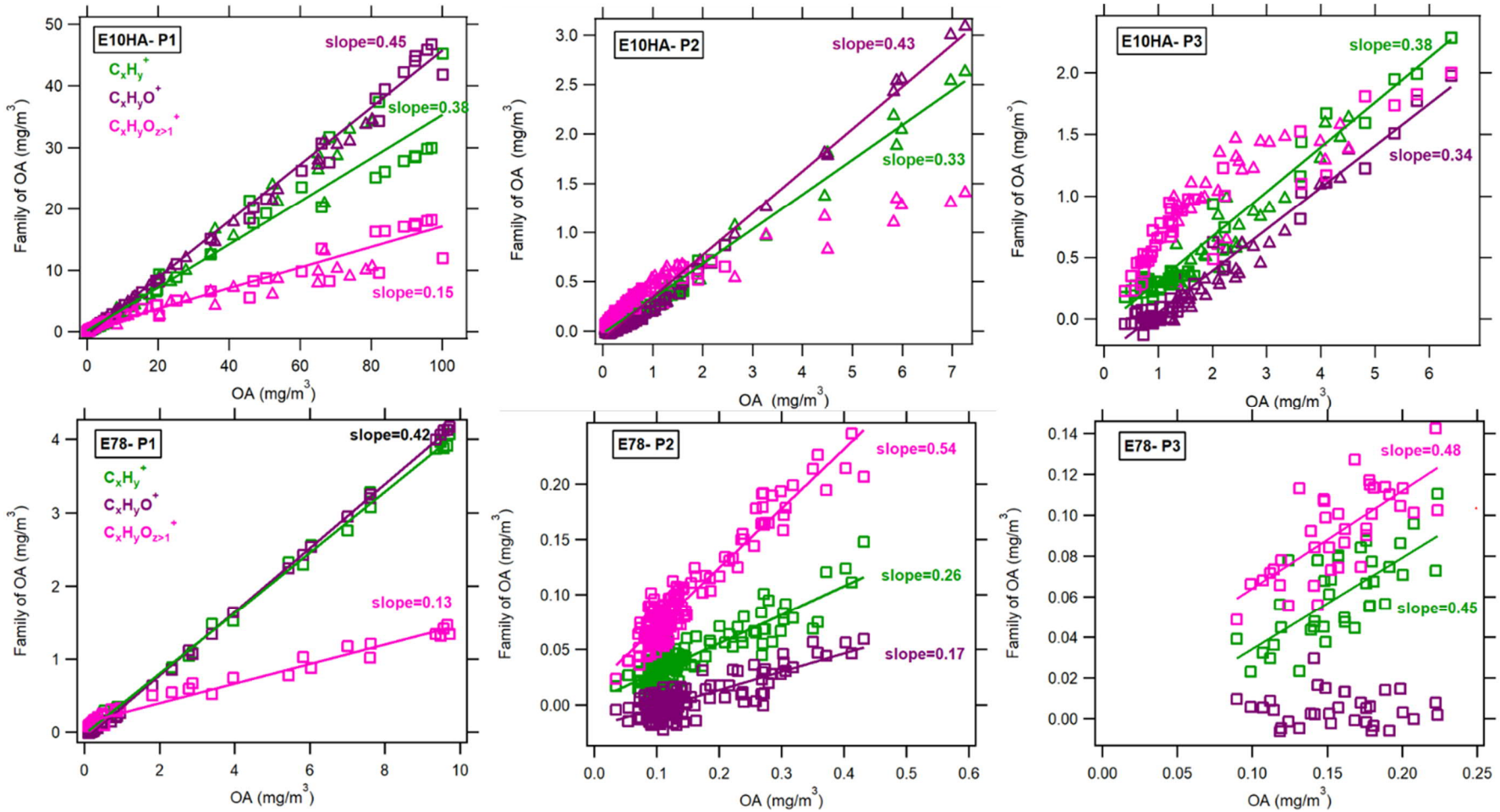

Figure 4: Relative contribution of different ion families to total OA for the LA92 cycle, using E10HA and E78 fuels. P1 is the cold-start phase, and P2 and P3 are the hot-running and hot-start phases, respectively

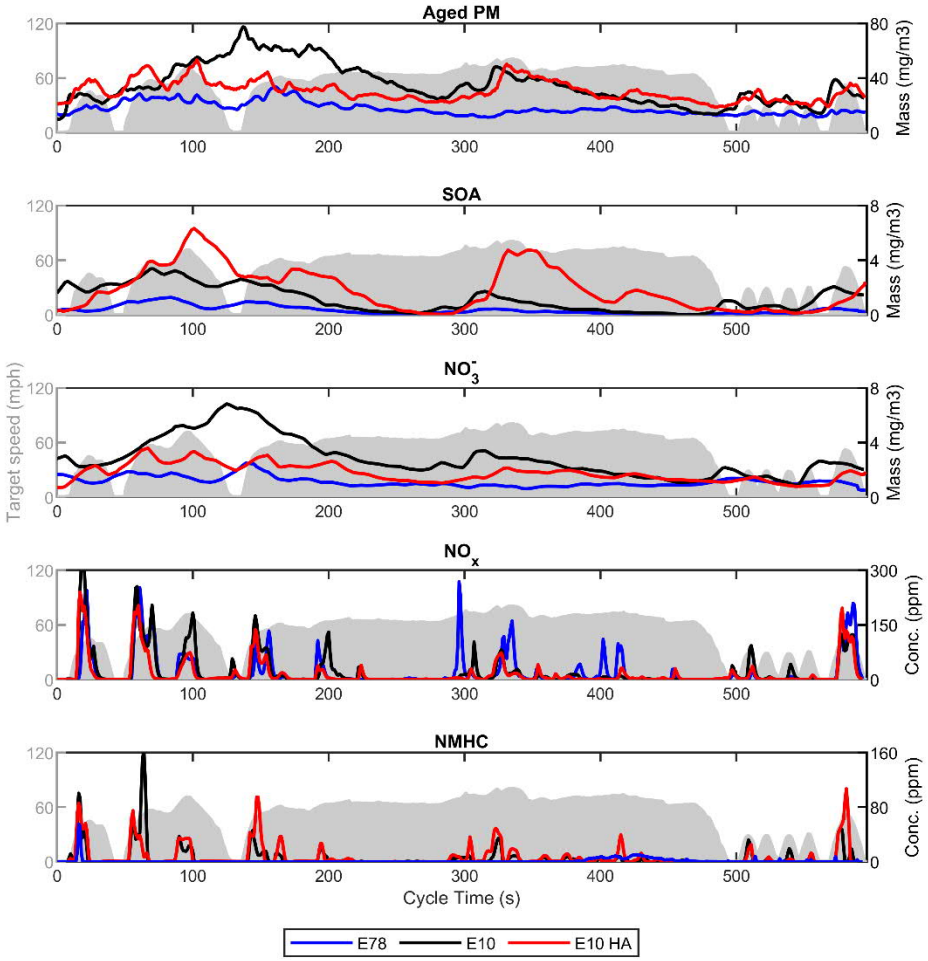

Figure 5: Aged PM, SOA, nitrate, NOx, and NMHC concentration over the US06 cycle with E10, E10HA, and E78. Note that NMHC concentrations for E78 were multiplied by a factor of 10. Shown concentrations have been corrected to represent tailpipe concentrations.

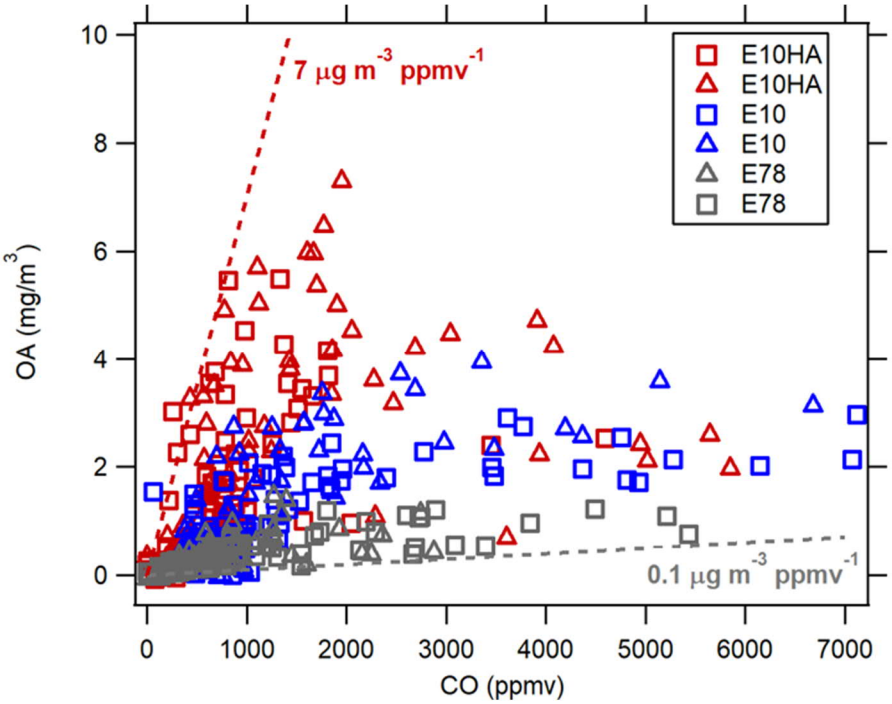

Figure 6: Correlation between measured OA and emitted CO for US06 runs on E10HA, E10, and E78 fuels. Different symbols of similar color present data from duplicate runs. The dashed lines represent the extreme boundaries of the data

Table 1: Cold-start and weighted gaseous and particulate emissions over the LA92 cycle

Emissions	E10	E10HA	E78
cold-start THC (g/mile)	0.42	1.94	2.33
weighted-THC (g/mile)	-	0.12	0.14
cold-start-NMHC (g/mile)	0.39	1.82	2.07
weighted-NMHC (g/mile)	-	0.11	0.11
cold-start-CO (g/mile)	2.05	7.54	8.57
weighted-CO (g/mile)		1.21	0.89
cold-start-NOx (g/mile)	0.08	0.13	0.57
weighted -NOx (g/mile)	-	0.03	0.05
cold-start-CO_2 (g/mile)	884.7	854.7	794.1
weighted -CO_2 (g/mile)	-	490.96	471.20
PM mass (mg/mile)	-	1.13	0.49
BC (mg/mile)	-	0.36	0.12
cold-start-TPN (#/mile)	1.55E+13	8.36E+13	3.40E+12
TPN (#/mile)	1.03E+12	5.47E+12	4.77E+11
cold-start-SPN (#/mile)	1.23E+13	1.06E+13	1.51E+12
SPN (#/mile)	7.49E+11	1.13E+12	2.71E+11

Table 2: Gaseous and particulate emissions over the US06 cycle

Emissions	E10	E10HA	E78
THC (g/mile)	0.07	0.06	0.00
NMHC (g/mile)	0.04	0.04	0.01
CO (g/mile)	2.35	2.00	1.58
NOx (g/mile)	0.09	0.07	0.12
CO_2 (g/mile)	342.13	328.69	325.17
PM mass (mg/mile)	2.99	2.56	5.61
BC (mg/mile)	0.41	0.47	0.46
TPN (#/mile)	7.17E+12	3.55E+05	1.16E+12
SPN (#/mile)	8.40E+11	-	6.84E+11